Interaction of spin-labeled HPMA-based nanoparticles with human blood plasma proteins – the introduction of protein-corona-free polymer nanomedicine

Klepac, Damir; Kostková, Hana; Petrova, Svetlana; Chytil, Petr; Etrych, Tomáš; Kereïche, Sami; Raška, Ivan; Weitz, David A.; Filippov, Sergey K.

Source / Izvornik: **Nanoscale, 2018, 10, 6194 - 6204**

Journal article, Published version
Rad u časopisu, Objavljena verzija rada (izdavačev PDF)

https://doi.org/10.1039/c7nr09355a

Permanent link / Trajna poveznica: https://urn.nsk.hr/urn:nbn:hr:184:909513

Nanoscale

PAPER

View Article Online
View Journal | View Issue

Cite this: *Nanoscale*, 2018, **10**, 6194

Interaction of spin-labeled HPMA-based nanoparticles with human blood plasma proteins – the introduction of protein-corona-free polymer nanomedicine†

Damir Klepac, *[a,b] Hana Kostková,[a] Svetlana Petrova, [a] Petr Chytil, [a] Tomáš Etrych, [a] Sami Kereïche,[c] Ivan Raška,[c] David A. Weitz [d] and Sergey K. Filippov *[a]

In this paper, we revised the current understanding of the protein corona that is created on the surface of nanoparticles in blood plasma after an intravenous injection. We have focused on nanoparticles that have a proven therapeutic outcome. These nanoparticles are based on two types of biocompatible amphiphilic copolymers based on *N*-(2-hydroxypropyl)methacrylamide (HPMA): a block copolymer, poly(ε-caprolactone) (PCL)-*b*-poly(HPMA), and a statistical HPMA copolymer bearing cholesterol moieties, which have been tested both *in vitro* and *in vivo*. We studied the interaction of nanoparticles with blood plasma and selected blood plasma proteins by electron paramagnetic resonance (EPR), isothermal titration calorimetry, dynamic light scattering, and cryo-transmission electron microscopy. The copolymers were labeled with TEMPO radicals at the end of hydrophobic PCL or along the hydrophilic HPMA chains to monitor changes in polymer chain dynamics caused by protein adsorption. By EPR and other methods, we were able to probe specific interactions between nanoparticles and blood proteins, specifically low- and high-density lipoproteins, immunoglobulin G, human serum albumin (HSA), and human plasma. It was found that individual proteins and plasma have very low binding affinity to nanoparticles. We observed no hard corona around HPMA-based nanoparticles; with the exception of HSA the proteins showed no detectable binding to the nanoparticles. Our study confirms that a classical "hard corona–soft corona" paradigm is not valid for all types of nanoparticles and each system has a unique protein corona that is determined by the nature of the NP material.

Received 15th December 2017,
Accepted 23rd February 2018

DOI: 10.1039/c7nr09355a

rsc.li/nanoscale

Introduction

For the delivery of drugs to a specific cell or organ, it is important to overcome the pharmacokinetic limitations associated with conventional drug formulations.[1] It was proved earlier that polymeric nanoparticles (NPs), *i.e.* self-assembled micelles composed of amphiphilic copolymers, could be successfully used as carriers for drug delivery.[2] These colloidal polymeric systems provide control over the drug's pharmacokinetics and biodistribution and at the same time improve the stability of the drug while it is delivered by the blood to the therapeutic place of action.[3,4] In addition, NPs can be designed to deliver many types of drugs by combining polymers of different structures, chemical compositions, hydrophilicities and charges.[3]

It is well known that there are more than 3700 proteins in blood and some of them bind to the surfaces of NPs immediately after injection of the materials into bloodstream, forming the so-called "protein corona".[5–15] This corona is the biological identity of a nanoparticle, as it is what the cell 'sees' and interacts with.[16] The interaction of drug delivery systems with blood proteins is therefore regarded as the most important issue that determines the nanoparticle stability, biodistribution, efficacy and toxicity.[7,17,18]

Nowadays, it is generally accepted that the protein corona has two shells: soft and hard coronas.[19] The hard corona consists of tightly bound proteins with higher affinity. These proteins cannot be removed from the NP surface even by strong agitation such as extensive centrifugation and washing. The soft corona is composed of proteins with lower affinity. It is

[a]*Institute of Macromolecular Chemistry, Czech Academy of Sciences, Heyrovsky Sq. 2, 162 06 Prague 6, Czech Republic. E-mail: damir.klepac@medri.uniri.hr, filippov@imc.cas.cz*
[b]*Faculty of Medicine, University of Rijeka, Braće Branchetta 20, 51000 Rijeka, Croatia*
[c]*Institute of Biology and Medical Genetics, First Faculty of Medicine, Charles University, Albertov 4, 128 01 Prague 2, Czech Republic*
[d]*Gordon McKay Laboratory, Harvard University, Oxford Street, Cambridge, MA 02138, USA*

†Electronic supplementary information (ESI) available: EPR simulation parameters, additional DLS data and cryo-TEM images, and a description of the basic characterization techniques. See DOI: 10.1039/c7nr09355a

believed that proteins in the soft corona are in dynamic equilibrium with the environment. It was Vroman and Adams who first discovered that the composition of proteins adsorbed on a surface changes with time.[20] More abundant plasma proteins like human serum albumin (HSA) are substituted with less abundant but more active proteins such as immunoglobulin G (IgG) and fibrinogens over time. Although it has not yet been proved experimentally, the Vroman effect should be valid for NPs as well. Nevertheless, a few reports have been published on nanoparticles with low or protein-free corona.[21,22] It was also established earlier that the absorption of proteins could be controlled by varying the composition of the copolymer.[23,24]

The real drawback of the vast majority of NPs whose interactions with blood plasma have already been reported in the literature is that they are not suitable for drug delivery. In this paper, we want to examine the protein corona of therapeutic NPs in blood plasma after an intravenous injection.

Despite the broad range of methodologies used to study NP–protein interaction, including UV-Vis,[25] fluorescence spectroscopy,[25] capillary electrophoresis,[26] the nanoparticle tracking analysis (NTA) method combined with field flow fractionation (FFF) and multi-angle light scattering (MALS),[27] dynamic light scattering (DLS),[28–31] isothermal titration calorimetry (ITC) and gel electrophoresis (SDS-PAGE),[6] and liquid chromatography (LC-MS/MS),[32] none of the abovementioned techniques can directly probe the dynamics of polymer chains in the NP hydrophobic core and hydrophilic shell during the interaction with proteins. Such dynamical changes could be a good marker of the protein presence on the NP surface.

Electron paramagnetic resonance (EPR) spectroscopy, however, is a powerful technique for studying the motion of nitroxyl radicals covalently attached to a molecule of interest. This technique is also known as "spin-labeling" and it has been successfully applied to study the dynamics of various polymer systems, proteins and lipids.[33,34] Li *et al.* have used the EPR technique to study the dynamic changes within telodendrimer-based NPs during interaction with blood proteins.[35] They found that the proteins and lipoproteins from blood plasma may influence the stability of NPs and rapidly destroy their structure. Additionally, they proposed that the stability of the investigated NPs could be improved by introducing disulfide cross-links in the core of NPs.[35]

Recently, we developed a new type of radical containing nanoparticle (RNP) based on poly[*N*-(2-hydroxypropyl)methacrylamide] (poly(HPMA)) as the hydrophilic block and a hydrophobic poly(ε-caprolactone) (PCL) block. These RNPs could potentially find applications as drug delivery systems and in the treatment of oxidative stress injuries.[36] The nitroxyl radicals located in a hydrophobic core of the NPs can be used as spin labels for EPR studies. Another type of nanoparticle containing amphiphilic HPMA copolymer bearing cholesterol as the hydrophobic moiety located along the hydrophilic polymer chain was developed previously.[37,38] Its conjugates with the anti-cancer drug doxorubicin, bound to the polymer carrier by a pH-sensitive bond, showed prolonged blood circulation, enhanced tumor uptake, controlled drug release in tumor tissue/cells and superior anticancer activity *in vivo*.

For EPR studies the NPs were covalently labeled with 2,2,6,6-tetramethylpiperidine-1-oxyl (TEMPO) radicals located at the end of the PCL block or randomly distributed along the hydrophilic HPMA copolymer chain.

The present study was aimed at investigating the influence of blood plasma and various plasma components on the chain dynamics in RNP containing the label in the hydrophobic PCL core or hydrophilic HPMA copolymer shell and verifying the validity of the classical "hard corona–soft corona" approach for HPMA copolymer-based NPs.

Experimental

Materials

Acetic acid, 1-aminopropan-2-ol, methacryloyl chloride, 6-aminohexanoic acid, methyl 6-aminohexanoate hydrochloride, hydrazine hydrate, cholesterol, *N*,*N*-diisopropylethylamine (DIPEA), 4,5-dihydrothiazole-2-thiol, dimethylacetamide (DMA), dimethyl sulfoxide (DMSO), ε-caprolactone (ε-CL, 99%), 2,2′-azobis(2-methylpropionitrile) (AIBN, 98%), 4-cyano-4-(thiobenzoylthio)pentanoic acid (CTA, >97%), 4-(dimethylamino)pyridine (DMAP, 99%), *N*,*N*′-dicyclohexylcarbodiimide (DCC, 99%), *m*-chloroperbenzoic acid (*m*CPBA, ≤77%) and tin(II) bis(2-ethylhexanoate) ($Sn(Oct)_2$, 95%, 0.06 M solution in toluene), 4-hydroxy-2,2,6,6-tetramethylpiperidine (TEMPH, 98%), 4-amino-TEMPO and 4-oxo-TEMPO (TEMPONE) were purchased from Sigma-Aldrich. High-density lipoprotein (HDL) and low-density lipoprotein (LDL) were purchased from Lee Biosolutions, Inc. (Maryland Heights, USA). Human plasma was obtained from the Military University Hospital in Prague from healthy donors. Human serum albumin (HSA), bovine serum albumin (BSA), immunoglobulin G (IgG), sodium dodecyl sulfate (SDS) and all other chemicals were purchased from Sigma-Aldrich.

Synthesis of monomers

N-(2-Hydroxypropyl)methacrylamide (HPMA) was synthesized according to the method of ref. 39. Cholest-5en-3β-yl 6-methacrylamido hexanoate (MA-Ahx-Chol) was prepared as described in ref. 37. 3-(3-Methacrylamidopropanoyl)thiazolidine-2-thione (MA-βAla-TT) was prepared as described in ref. 40. 6-Methacrylamido hexanoyl hydrazine (MA-Ahx-$NHNH_2$) was synthesized as described in ref. 41.

Synthesis of spin-labeled PCL-*b*-poly(HPMA) diblock copolymer

A detailed synthetic procedure for TEMPO-PCL-*b*-poly(HPMA) (copolymer **1**) (Scheme 1) is described in our previous publication.[36] Briefly, α-2,2,6,6-tetramethylpiperidin-ω-hydroxy-PCL prepolymer (α-TEMP-PCL) was obtained *via* ring-opening polymerization (ROP) of ε-CL initiated by 4-hydroxy-2,2,6,6-tetramethylpiperidine. In the second step, the PCL-CTA macromolecular chain transfer agent (PCL macroCTA agent) was prepared from

α-TEMP-PCL in high yield by using the carbodiimide chemistry (DCC) method. The resulting PCL macroCTA agent was applied in the third reaction step under reversible addition–fragmentation chain transfer (RAFT) polymerization conditions to supply the PCL-*b*-poly(HPMA) diblock copolymers. In the last step, oxidation by *m*-chloroperbenzoic acid of 2,2,6,6-tetramethylpiperidine groups in the composition of the diblock copolymers afforded the corresponding stable TEMPO radicals. The copolymer **1** was used for the preparation of RNP containing the label in the hydrophobic core (RNP-C).

Synthesis of spin-labeled HPMA copolymers bearing cholesterol

Two types of random HPMA copolymers differing in the spacer length between the spin probe and the polymer carrier chain were synthesized. Their physico-chemical characteristics are showed in Table 1.

The polymer poly(HPMA-*co*-MA-Ahx-Chol-*co*-MA-Ahx-TEMPONE) (copolymer **2**) bearing cholesterol and TEMPONE was synthesized by a two-step synthesis: Firstly, the terpolymer poly(HPMA-*co*-MA-Ahx-Chol-*co*-MA-Ahx-$NHNH_2$) was prepared by free radical polymerization of HPMA, MA-Ahx-Chol and MA-Ahx-$NHNH_2$ in methanol using AIBN as the initiator and purified according to ref. 37. Afterwards, TEMPONE was bound to the polymer carrier *via* a hydrazone bond with the following procedure: 340 mg of the polymer poly(HPMA-*co*-MA-Ahx-Chol-*co*-MA-Ahx-$NHNH_2$) and 3.4 mg of TEMPONE were dissolved in 3.3 mL of methanol and 132 μL of acetic acid was added into the stirred solution. After 24 h-reaction at 25 °C the polymer conjugate was purified from low molecular weight impurities by gel filtration (Sephadex LH-20; methanol as the solvent) and isolated by precipitation in ethyl acetate, filtered and dried to constant weight. The yield was 295.6 mg (86.9%). The copolymer **2** was used for the preparation of RNP containing the label in the hydrophilic shell bound by a longer spacer (RNP-Sl).

The polymer carrier poly(HPMA-*co*-MA-Ahx-Chol-*co*-MA-βAla-TEMPO) (copolymer **3**) bearing cholesterol and 4-amino-TEMPO attached *via* an amide bond was prepared by a two-step synthesis: firstly, the terpolymer of HPMA, MA-Ahx-Chol and MA-βAla-TT (poly(HPMA-*co*-MA-Ahx-Chol-*co*-MA-βAla-TT)) was prepared by free radical polymerization in DMSO using AIBN as the initiator (AIBN (2 wt%); monomers (18 wt%); molar ratio of HPMA: MA-Ahx-Chol : MA-βAla-TT of 93 : 2 : 5). The resulting polymer was isolated by precipitation in a mixture of acetone and diethyl ether 2 : 1, dissolved in methanol and reprecipitated in acetone, washed with diethyl ether, filtered and dried to constant weight. Then 4-amino-TEMPO was bound to the polymer carrier by aminolysis of the polymer thiazoline-2-thione (TT) groups: 59.3 mg of the polymer poly (HPMA-*co*-MA-Ahx-Chol-*co*-MA-βAla-TT) and 2 mg of 4-amino-TEMPO were dissolved in a mixture of 600 μL DMA and 400 μL methanol with 30 μL of DIPEA. The reaction proceeded at 25 °C and after 2 h the polymer conjugate was purified from low molecular weight impurities by gel filtration (Sephadex LH-20; methanol solvent) and isolated by precipitation in ethyl acetate, filtered and dried to constant weight. The yield was 42.1 mg (68.7%). The copolymer **3** was used for the preparation of RNP containing the label in the hydrophilic shell bound by a shorter spacer (RNP-Ss).

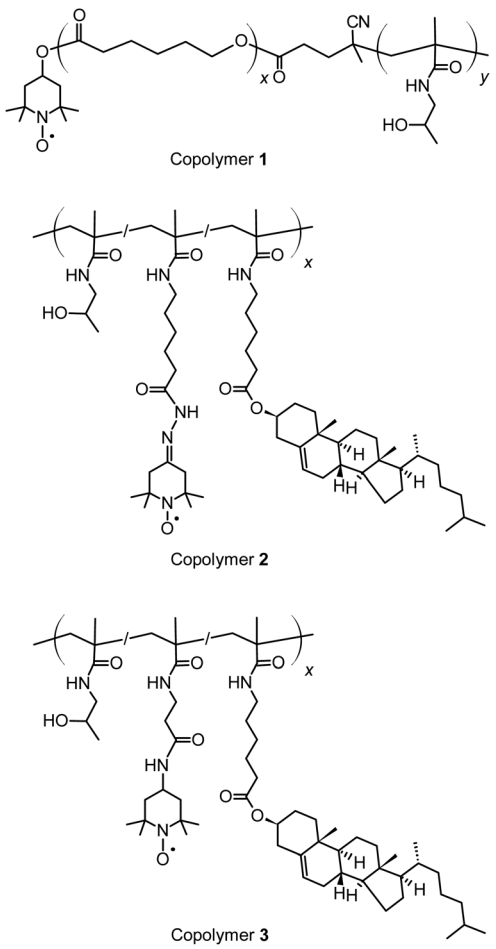

Scheme 1 Schematic structures of copolymers **1–3**.

Preparation of the nanoparticles

The core–shell RNPs were prepared by the nanoprecipitation method.[42] Copolymers **1–3** (20 mg) were dissolved in dimethylformamide (DMF) (6 mL). The solutions were then injected dropwise using a syringe (G = 26) into phosphate-buffered saline (PBS, pH 7.4) (14 mL) while stirring magnetically at room temperature. The organic solvent was removed *via* dialysis in PBS over 24 h using a 3–5 kDa molecular weight cut-off membrane. The final concentration of both types of NPs was 1.0 mg mL^{-1}.

Characterization techniques

Electron paramagnetic resonance (EPR) spectroscopy. A solution of spin-labeled NPs (1.0 mg mL^{-1}) was mixed with SDS, HSA, BSA, HDL, LDL, IgG and human plasma. The final concentrations of the proteins were comparable to the levels usually present in human blood (50 mg mL^{-1} for HSA and BSA, 2 mg mL^{-1} for HDL and LDL and 10 mg mL^{-1} for IgG).

Table 1 Physico-chemical characteristics of spin-labeled copolymers

Sample	Structure	M_w[a] (g mol^{-1})	$Đ$[a]	Content of cholesterol[b] (mol%)	Content of probe[c] (mol%)
Copolymer **1**	TEMPO-PCL-*b*-poly(HPMA)	44 000	1.4	N/A	0.50
Copolymer **2**	Poly(HPMA-*co*-MA-Ahx-Chol-*co*-MA-Ahx-TEMPONE)	27 500	2.3	2	0.03
Copolymer **3**	Poly(HPMA-*co*-MA-Ahx-Chol-*co*-MA-βAla-TEMPO)	25 000	1.6	2	0.02

[a] Molecular weights (M_w) and dispersity ($Đ$) were determined by GPC with MALS detection. [b] The content of cholesterol was determined by ^{1}H-NMR spectroscopy. [c] The content of the spin probe was determined by UV-Vis spectroscopy.

EPR measurements were performed using a 20 μL capillary on a Bruker ELEXSYS E-540 X-band spectrometer equipped with a Bruker ER 049X microwave bridge and a Bruker ER4131VT variable temperature unit. Spectra were recorded at 37 °C with a sweep width of 100 G, a microwave power output of 6 mW, a modulation frequency of 100 kHz, and a sweep time of 22 minutes to improve the signal-to-noise ratio. The modulation amplitude was optimized to the line width of the spectrum (of the order of 1.0 to 2.0 G).

EPR simulations. The spectra were simulated using the spectral fitting program NLSL, which is based on the stochastic Liouville equation and utilizes the modified Levenberg–Marquardt minimization algorithm to calculate the best fit with experimental spectra.[43] The spin label motion was assumed to follow the Brownian diffusion model with an axially symmetric rotational diffusion tensor. The components of the **g** and **A** tensors were determined by analyzing the rigid limit spectra. All spectra were simulated with a single spectral component. The fits were obtained by varying the parallel and perpendicular rotational diffusion coefficients (R_{prp}, R_{pll}), the diffusion tilt angle (β_D) and the inhomogeneous line width tensor (W_1). The quality of the fit was determined by the correlation coefficient r, which was above 0.99 for all fits.

Rotational correlation times (τ_R) were calculated using eqn (1):[43]

$$\tau_R = \frac{1}{6\sqrt[3]{R_{prp}{}^2 R_{pll}}} \quad (1)$$

Dynamic light scattering (DLS). The DLS measurements were performed using an ALV CGE laser goniometer. The scattered light of a 22 mW HeNe linear polarized laser (632.8 nm) was collected using an ALV 6010 correlator in a broad angle range of 40–150°. The DLS experiments were conducted at body temperature, T = 37 °C. Counting times were varied in the range of 100 to 300 s to accumulate an intensity correlation function $g_2(t)$ with a high signal-to-noise ratio. The measured $g_2(t)$ was analyzed using the algorithm REPES (incorporated into the GENDIST program), resulting in a distribution of relaxation times τ, $A(\tau)$. The translational diffusion coefficient D_{tr} was obtained using the equation:

$$\Gamma = \tau^{-1} = D_{tr} q^2 \quad (2)$$

where Γ is the relaxation rate, $q = 4\pi n \sin(\theta/2)/\lambda$ is the magnitude of the scattering vector with λ corresponding to the laser wavelength, n is the refractive index of the solvent, and θ is the scattering angle.

The apparent hydrodynamic radius (R_h) of the NPs was calculated using the Stokes–Einstein equation:

$$R_h = \frac{k_B T}{6\pi D_{tr}} \quad (3)$$

where k_B is the Boltzmann constant, T is the absolute temperature, η is the viscosity of the solvent, and D is the apparent diffusion coefficient of the NPs.

Cryo-transmission electron microscopy (cryo-TEM). Cryo-TEM measurements were carried out using a Tecnai G^2 Sphera 20 electron microscope (FEI Company, Hillsboro, OR, USA) equipped with a Gatan 626 cryo-specimen holder (Gatan, Pleasanton, CA, USA) and a LaB_6 gun. The samples for cryo-TEM were prepared by plunge-freezing.[44] Briefly, 3 μL of the sample solution was applied to a copper electron microscopy grid covered with a perforated carbon film forming woven-mesh-like openings of different sizes and shapes (the lacey carbon grids #LC-200 Cu, Electron Microscopy Sciences, Hatfield, PA, USA) and then glow discharged for 40 s with 5 mA current. Most of the sample was removed by blotting (Whatman No. 1 filter paper) for approximately 1 s, and the grid was immediately plunged in liquid ethane held at −183 °C. The grid was then transferred without rewarming to the microscope. Images were recorded at an accelerating voltage of 120 kV and magnifications ranging from 11 500× to 50 000× using a Gatan UltraScan 1000 slow scan CCD camera in the low-dose imaging mode, with an electron dose not exceeding 1500 electrons per nm^2. The magnifications resulted in final pixel sizes ranging from 1 to 0.2 nm, and the typical value of the applied underfocus ranged from 0.5 to 2.5 μm. The applied blotting conditions resulted in specimen thicknesses varying between 100 and *ca.* 300 nm. Brightness and contrast corrections of the acquired images were performed using the ImageJ software.

Isothermal titration calorimetry (ITC). The isothermal titration microcalorimetry experiments were performed using a MicroCal ITC_{200} calorimeter. The experiment was performed with consecutive injections of the protein solution into the measurement cell; the cell contained 280 μL of the polymer solution or water. A protein solution was added into a 40 μL injection syringe, which also acted as a stirrer. The stirring speed was in the range of 500–1000 rpm. The injection volume was 2 μL. The time between injections was usually 200 s. The

measurements were recorded at 37 °C. The data were analyzed using the MicroCal Origin software. The experimental value of enthalpy (ΔH) was obtained by integrating the raw data signal, and the integrated molar enthalpy change per injection was obtained by dividing the experimentally measured enthalpy by the number of moles of protein added. The final data are the plots of the integrated molar enthalpy change as a function of the total protein concentration in the calorimeter sample cell.

Results and discussion

Behavior of nanoparticles in phosphate-buffered saline (PBS)

Spin-labeled NPs bearing the probe in the hydrophobic core (RNP-C) (Fig. 1(a)) were self-assembled from PCL-*b*-poly (HPMA) diblock copolymers labeled with TEMPO radicals at the end of the hydrophobic PCL block (copolymer **1**). After micellization, the TEMPO radicals were located in the hydrophobic core of the NPs and closely followed the dynamics of the PCL chain.[36] Two variants of the spin-labeled NPs bearing the probe in the hydrophilic shell bound by a longer (RNP-Sl) or a shorter spacer (RNP-Ss) (Fig. 1(b) and (c)) were prepared from the corresponding copolymers **2** and **3** with different spacer lengths between the spin probe and the polymer carrier. Here, the NPs were labeled with 4-oxo- (RNP-Sl) or 4-amino-TEMPO radicals (RNP-Ss) randomly distributed along the hydrophilic HPMA copolymer chain. The spacers between the spin label and the HPMA copolymer backbone were composed of two or five methylene groups for RNP-Ss or RNP-Sl, respectively. Although the TEMPONE spin probe was bound by the hydrazone bonds, which can be potentially hydrolytically labile, we observed not more than only 6% of the released probe after 24 h at 37 °C in a phosphate buffer of pH 7.4. Thus, the differences in properties of RNP-Ss and RNP-Sl described below can be ascribed only to the spacer length.

Dynamic light scattering shows that copolymer **1** forms NPs (RNP-C) in PBS with a hydrodynamic radius of ~43 nm with sharp distribution, whereas copolymer **3** self-assembles to form NPs (RNP-Ss) with a comparable average radius of 40 nm but a broader distribution (Fig. S1†).

To evaluate the capability of the spin label to provide information about the motion of the outer hydrophilic shell of the RNP-Ss or RNP-Sl NPs and the inner hydrophobic PCL core of RNP-C NPs, we compared the EPR spectra obtained from RNP-C, RNP-Ss and RNP-Sl with the spectra of pure TEMPONE radicals (Fig. 2).

The characteristic three-line EPR signal of the nitroxyl radical arises due to anisotropic hyperfine interactions between the unpaired electron and the nitrogen nucleus.[45] The narrow EPR lines of almost equal intensities observed for pure TEMPONE are characteristic of very fast motions of the nitroxyl radical in the PBS solution. The EPR spectrum of RNP-Sl is very similar to that of pure TEMPONE except for its high field line, which has a lower intensity due to the slightly

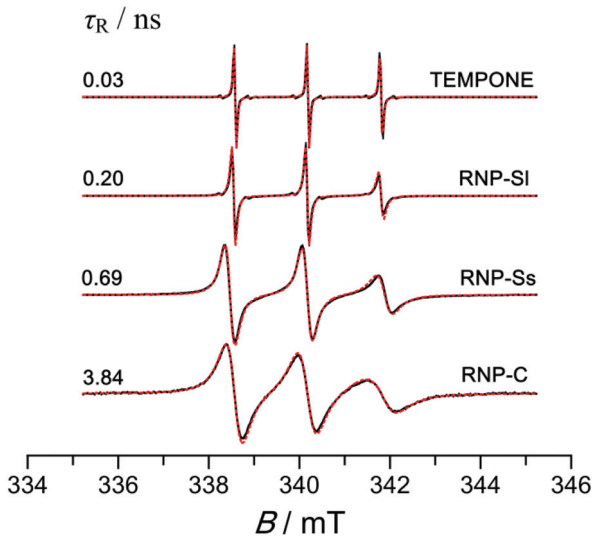

Fig. 2 EPR spectra of pure TEMPONE, RNP-Sl, RNP-Ss and RNP-C in PBS at 37 °C. Solid lines represent experimental spectra, and dotted red lines represent simulated spectra.

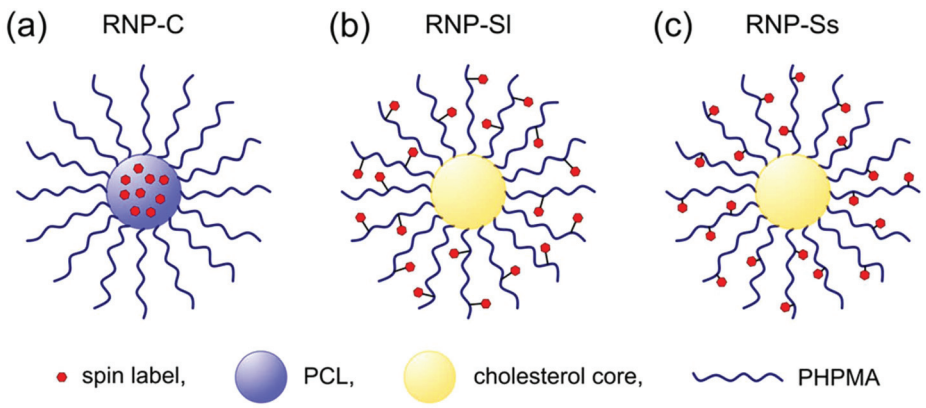

Fig. 1 Schematic representation of spin-labeled NPs containing the spin label (a) in the hydrophobic core (RNP-C), (b) in the hydrophilic shell *via* a longer spacer (RNP-Sl) and (c) in the hydrophilic shell *via* a shorter spacer (RNP-Ss).

slower (restricted) mobility of the attached nitroxyl radical. However, the EPR spectrum observed for the RNP-Ss is considerably broader (Fig. 2). This broadening of the EPR signal reflects the slower spin label mobility in RNP-Ss when compared to both TEMPONE and RNP-Sl. On the other hand, the EPR spectrum of RNP-C is the broadest one due to the significantly restricted motional freedom of the nitroxyl radical (Fig. 2). This mobility can be quantified by the rotational correlation time, τ_R, which corresponds to the average time during which a radical rotates by one radian. To extract rotational correlation times, we simulated and compared the EPR spectra obtained at 37 °C. The parameters used for the EPR spectral fitting and calculated rotational correlation times are given in Table S1.†

The simulated EPR spectra of pure TEMPONE, RNP-Sl, RNP-Ss and RNP-C in PBS at 37 °C are shown as dotted red lines in Fig. 2. The τ_R values of 0.20 and 0.69 ns obtained for RNP-Sl and RNP-Ss (Fig. 2, dotted red lines, Table S1†) confirm that the spin label mobility falls under the fast motional regime (10^{-11} to 10^{-9} s) where the spectral changes are very sensitive to molecular motion.[46] This is not surprising since the radicals are attached to the outer hydrophilic HPMA copolymer shell of RNP-Ss and RNP-Sl through a flexible spacer. The mobility of the spin label in RNP-Ss and RNP-Sl is therefore only partially restricted by the HPMA copolymer chains.

τ_R of a spin label attached to a poly(HPMA) backbone with the spacer composed of five methylene groups (RNP-Sl) increased more than six times compared to the free TEMPONE radical in PBS solution (from 0.03 ns to 0.20 ns). The longer correlation time indicates the slower dynamics of the spin label after attachment to the polymer backbone. By shortening the spacer length between the spin label and HPMA copolymer chain (RNP-Ss) the correlation time additionally increased to 0.69 ns (23 times compared to the free TEMPONE). The same behavior was observed in proteins where the correlation time of the unbound, free label in aqueous solution increased from ~0.05 ns to 0.80 ns after attachment to a soluble protein fragment.[47,48] These results are in good agreement with a previous study by Pilar *et al.*, who found that the correlation time of the spin label attached to a methacrylamide-based copolymer decreases monotonically with increasing side chain length.[49]

In the case of RNP-C, the calculated τ_R value of 3.84 ns (Fig. 2, dotted red line, Table S1†) indicates that the spin label mobility is much more restricted compared to the label in RNP-Ss and RNP-Sl. Since the spin labels in RNP-C are attached to the end of the hydrophobic PCL chains, after the self-assembly process they become located in the cores of NPs where their mobility is significantly constrained by the dense hydrophobic environment.

The spin label mobility depends on the flexibility of the spacer that connects it to the backbone and on the motions of the entire macromolecule. To study the dynamics of the HPMA copolymer chains during interaction with proteins it is necessary to minimize the influence of the internal motions of the nitroxide radical about the chemical bonds of the spacer. Therefore, NPs with shorter spacer length between the spin label and the HPMA polymer carrier (RNP-Ss) were chosen for all subsequent measurements. The rotational correlation time, τ_R, can be used as a sensitive parameter to detect the presence of a protein corona on the surface of the NPs.

Effect of sodium dodecyl sulfate on nanoparticles

To verify the sensitivity of the EPR method, we explored the behavior of NPs in the presence of sodium dodecyl sulfate (SDS), a highly effective anionic surfactant commonly used for protein denaturation. SDS molecules attach to proteins mainly by hydrophobic interactions inducing unfolding of the protein tertiary structure. The driving force for this extension arises from repulsions between the SDS molecules and negatively charged side chains of the protein.[50] Cryo-TEM and dynamic light scattering (DLS) results (Fig. 3 and S2†) clearly show that the structure of RNP-C and RNP-Ss become disrupted in the presence of SDS. For both types of NPs the mode from NPs disappears and two peaks are manifested on a distribution function instead. The slow mode corresponds to the SDS micelles, whereas the second peak could be attributed to the aggregates of SDS and polymeric unimers.

The changes in EPR spectra of RNP-C and RNP-Ss after interaction with SDS are shown in Fig. 4.

The EPR spectrum of RNP-C in SDS (2.0 mg mL^{-1}) shows significantly narrower lines compared to the spectrum in PBS. When the structure of RNP-C is disrupted by SDS, the spin labels which were tightly arranged in the dense hydrophobic core suddenly become exposed to the solution where they have much higher mobility.

The calculated τ_R values (Fig. 4(a), Table S2†) show that the mobility of spin labels in RNP-C increases by an order of magnitude after interaction with SDS. In the case of RNP-Ss,

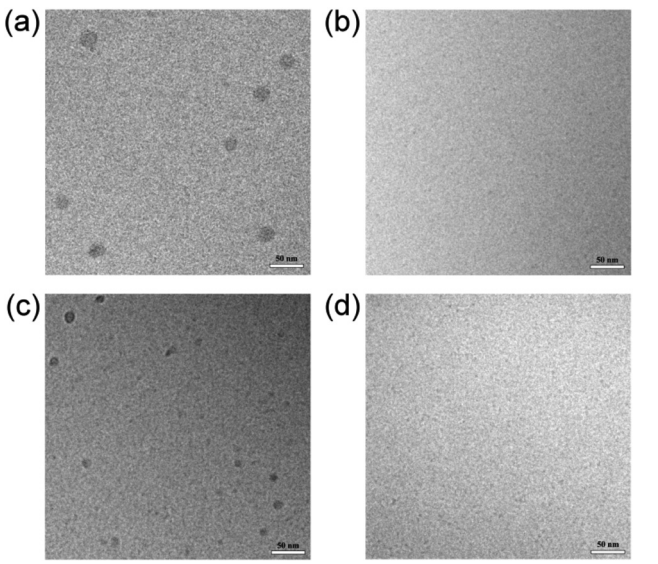

Fig. 3 Cryo-TEM images of (a) RNP-C in PBS (b) RNP-C in the presence of 2.0 mg mL^{-1} SDS, (c) RNP-Ss in PBS and (d) RNP-Ss in the presence of 2.0 mg mL^{-1} SDS.

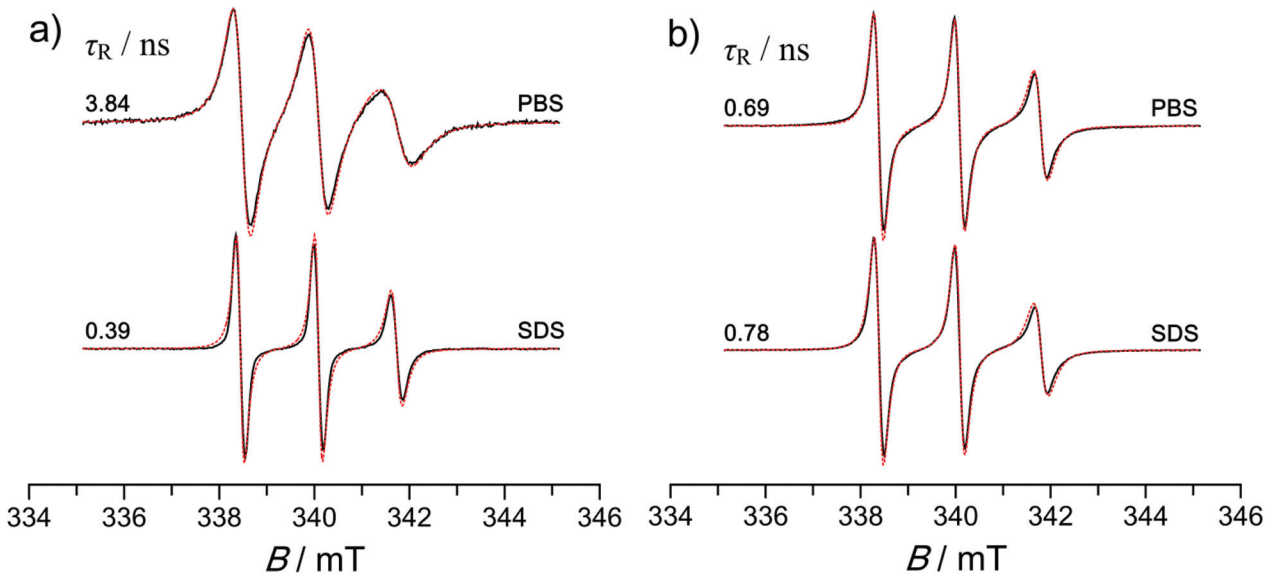

Fig. 4 EPR spectra of (a) RNP-C and (b) RNP-Ss in PBS with and without SDS (c = 2.0 mg mL^{-1}) at 37 °C. Solid lines represent experimental spectra, and dotted red lines represent simulated spectra.

however, no spectral changes are observed after interaction with SDS and the spectral simulations show only a minor change in the calculated τ_R values (Fig. 4(b), Table S2†). Clearly, the disruption of RNP-Ss is not reflected in the EPR spectrum since the spin labels attached on the surface of these NPs already show relatively high mobility even before disintegration. The same effect was observed for non-cross-linked NPs assembled from amphiphilic telodendrimers.[35] We also investigated the changes in EPR spectra of RNP-C after treatment with different concentrations of SDS. As shown in Fig. 5(a), the relatively broad spectrum of RNP-C in PBS solution (0.00 mg mL^{-1} of SDS) gradually narrows with increasing SDS concentration until finally reaching the shape characteristic of fast motion in 2.00 mg mL^{-1} SDS solution. Simulations reveal that the τ_R values for labels in RNP-C decrease exponentially with increasing SDS concentration (Fig. 5(b), Table S3†). Clearly, 1.0 mg mL^{-1} of SDS is already sufficient to completely disintegrate the structure of the investigated NPs.

To improve the stability of nanoparticle micelles several techniques such as stereocomplexation,[51] non-covalent interactions[52,53] and crosslinking[54–56] have previously been applied. Crosslinked NPs were found to be resistant to SDS disruption.[35,57,58] Such modifications, however, are not always possible and it is imperative to investigate the stability of the prepared NPs in a real blood environment to assess the need for additional stabilization.

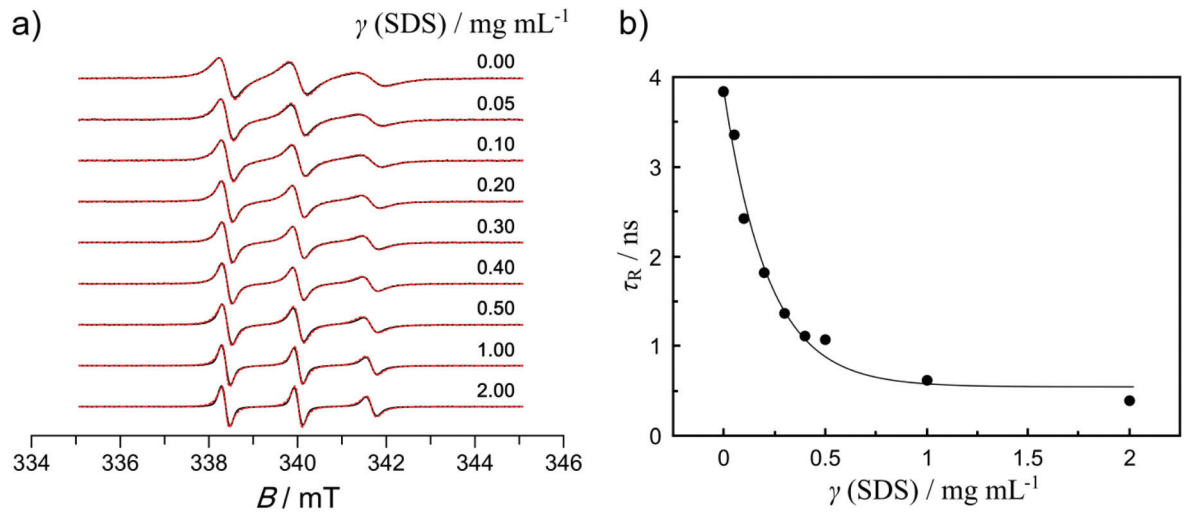

Fig. 5 (a) EPR spectra of pure RNP-C in PBS as a function of SDS concentration at 37 °C. Solid lines represent experimental spectra, and dotted red lines represent simulated spectra. (b) The dependence of rotational correlation time on SDS concentration at 37 °C in PBS.

Interaction of nanoparticles with proteins

To investigate the interaction of various blood plasma proteins with RNP-C and RNP-Ss the NPs were incubated in HSA, bovine serum albumin (BSA), high-density lipoprotein (LDL), low-density lipoprotein (LDL), IgG and human plasma for 1 h and the EPR spectra were recorded at 37 °C. The concentrations of proteins and lipoproteins were comparable to their typical blood levels.[59–61] The simulated EPR spectra of RNP-C and RNP-Ss in PBS, plasma and various plasma proteins are shown together with recorded EPR spectra in Fig. 6.

Human serum albumin (HSA) is the most abundant protein in plasma and it affects the pharmacokinetics of many drugs due to its extraordinary ligand-binding capacity.[62] It is generally the first protein that is adsorbed and for this reason it can strongly influence *in vivo* NP biodistribution.[5,63] However, the shape of the EPR spectra of RNP-Ss after incubation with HSA and BSA is the same as the spectrum in pure PBS (Fig. 6(b)). This observation is also evident by comparing the corresponding rotational correlation times (Fig. 6(b), Table S5†). These results indicate that HSA and BSA do not significantly bind to the outer HPMA copolymer shell of RNP-Ss and the protein corona is not formed. Moreover, the τ_R values for RNP-C remain essentially unchanged after incubation with HSA and BSA (Fig. 6(a), Table S4†), indicating that serum albumins are not able to penetrate the poly(HPMA) shell and enter the PCL core where they could influence the mobility of spin labels. This behavior is consistent with previous studies on telodendrimer-based NPs having polyethylene glycol (PEG) in the surface.[35] The same study by Li *et al.* has also demonstrated that lipoprotein particles, particularly LDL, can interact with the non-cross-linked NPs composed of a PEG shell and disrupt their assembly structure rapidly. It was proposed that lipoprotein particles and micellar NPs are likely to exchange contents with each other due to the similar amphiphilic nature causing the disassembly of the NPs.[35] To overcome this effect the NPs were additionally stabilized by introducing disulfide cross-links within the core.[58] Such micelles exhibit superior structural stability compared to their non-cross-linked counterparts[64–66] and can better retain their assembly structure in the presence of blood proteins.[35] However, to release the drug payload the intra-micellar disulfide bonds should first be cleaved by a reducing agent, which could be inconvenient in some therapeutic cases. Contrarily, we found that the shape of the EPR spectra and calculated correlation times remained unchanged after incubation of RNP-Ss and RNP-C in LDL and HDL compared to the spectra in PBS (Fig. 6, Tables S4 and S5†). These results indicate that the lipoproteins (HDL and LDL) are not able to bind or penetrate the hydrophilic shell of NPs such as RNP-Ss and RNP-C and the micelles could retain their structural integrity even without additional crosslinking. This can be explained by the unique structure of HPMA copolymers. In contrast with PEG, HPMA has lower propensity to form hydrogen bonds and therefore no interactions are possible between the HPMA copolymer shell and proteins and lipoproteins. Cukalevski *et al.* recently found that immunoglobulin G (IgG), the main type of antibody found in blood, enhances the aggregation of polystyrene NPs by forming protein bridges between them.[67] Our EPR results, however, show that even if the bridges are formed at the surface of HPMA copolymer based NPs they do not make strong enough connections with HPMA polymer chains to influence their mobility (Fig. 6(b), Table S5†). Finally, we investigated how the human plasma influences chain dynamics in HPMA copolymer based NPs. Again, it can be seen (Fig. 6, Tables S4 and S5†) that the mobility of the spin labels in RNP-C and RNP-Ss was not affected by

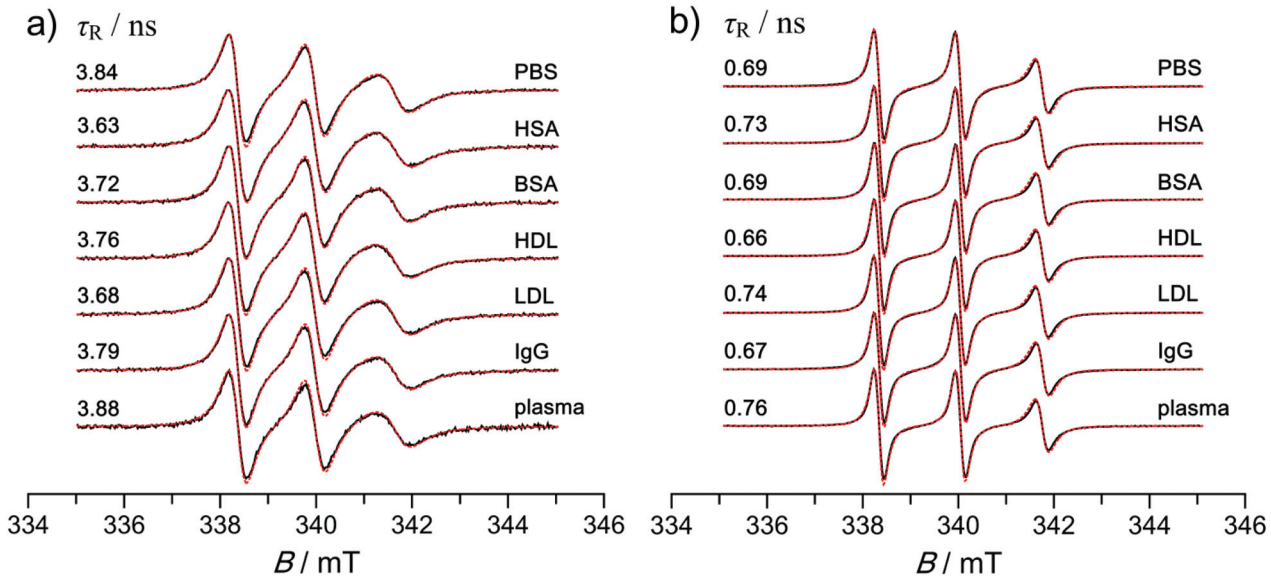

Fig. 6 EPR spectra of (a) RNP-C and (b) RNP-Ss in PBS and in the presence of different proteins at 37 °C in PBS. Solid lines represent experimental spectra, and dotted red lines represent simulated spectra.

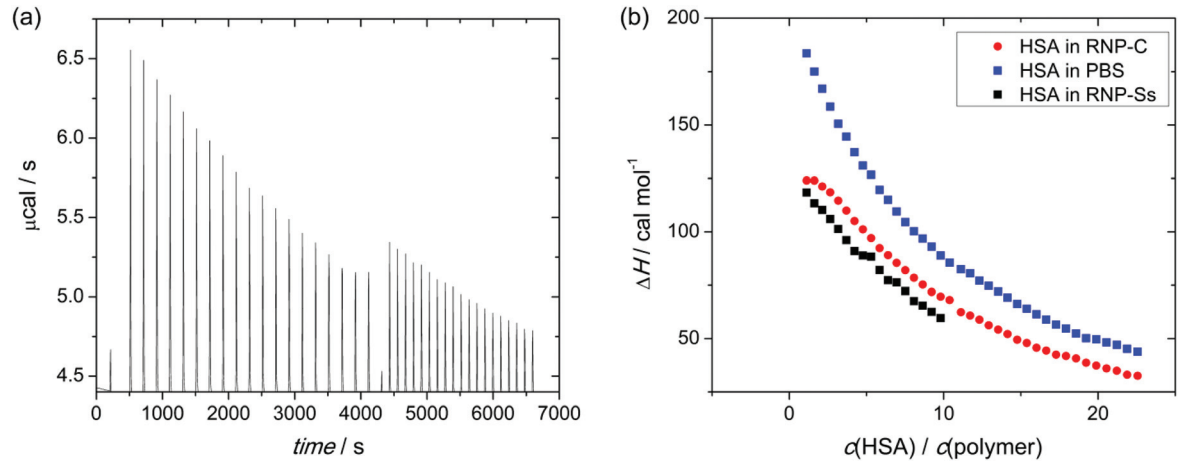

Fig. 7 ITC experiments: (a) the heat flow per injection in the titration of HSA (c = 50 mg mL^{-1} in PBS) into PBS. (b) Observed enthalpy changes for the titration of HSA (c = 50 mg mL^{-1}) into RNP-C (1 mg mL^{-1} in PBS) and RNP-Ss (1 mg mL^{-1} in PBS). T = 37 °C.

human plasma. This finding is in contrast with previously published results on PEG based NPs whose assembly order was immediately lost after incubation in human plasma as reflected in the sharper EPR spectrum.[35]

To verify the conclusions obtained from our EPR studies, two complementary methods were exploited. Since HSA is the most abundant protein in blood plasma, ITC experiments were performed to check its binding affinity to RNP-C and RNP-Ss NPs. A blank experiment with titration of HSA solution into PBS shows endothermic peaks whose amplitude decreases with increasing HSA concentration in solution (Fig. 7(a)). Such behavior is usually observed for dilution experiments of polymers and proteins. Titration of HSA into RNP-C and RNP-Ss shows only minor changes in comparison with the blank experiment (Fig. 7(b)). There is no strong adsorption of HSA on the nanoparticle surface, which is in agreement with the EPR results presented above. The small mismatch between curves could be attributed to insignificant interactions of HSA with polymers resulting in the formation of the thin layer of HSA that exists in dynamic equilibrium with polymer chains.

One might expect that the presence of a thick corona could be recognized by the distribution function of R_h in DLS experiments since larger objects, with scattered intensity proportional to the sixth power of size, scatter more effectively than small entities. Closer inspection of distribution functions shows no significant difference between the distribution functions of each particular protein and the solution in the presence of polymer NPs (Fig. 8(a) and (b)).

We explain these findings by the presence of large protein aggregates that suppress the scattering from NPs. Such a conclusion is in agreement with cryo-TEM results (Fig. S3–S6†), where polydisperse aggregates are clearly visible.

With these results from EPR, ITC, and DLS methods it is possible to conclude that blood plasma proteins form no hard corona around HPMA based NPs. This result is in perfect agreement with *in vivo* testing of drug carriers based on amphiphilic HPMA polymer conjugates with doxorubicin.[37]

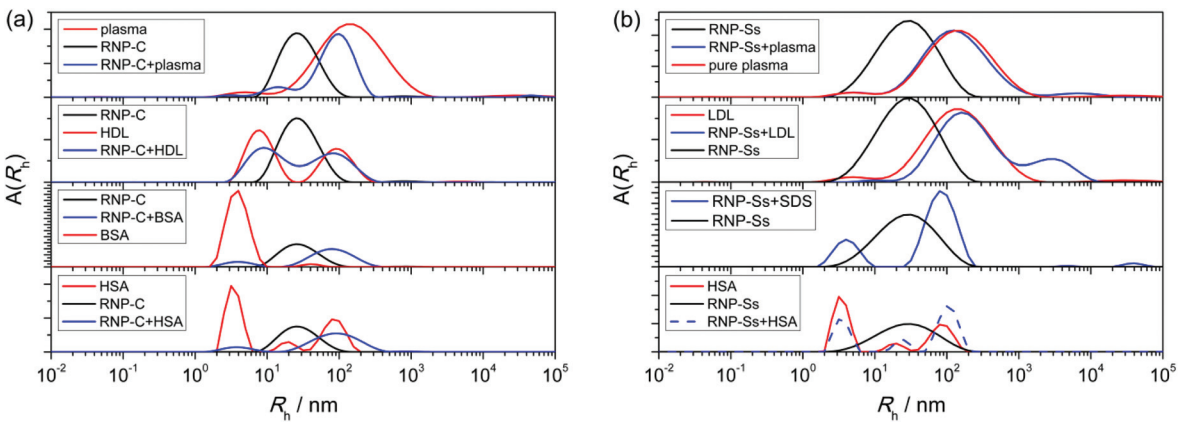

Fig. 8 Distribution functions A(R_h) for (a) RNP-C and (b) RNP-Ss in the presence of different proteins. The distribution functions of pure proteins and pure NPs in solution are presented for comparison.

Indeed, HPMA copolymers provide perfect "stealth" properties to NPs, preventing them from interaction with human blood plasma proteins and, thus, keeping their functionality unchanged. All previous publications where "hard corona–soft corona" was reported should be reevaluated now with respect to the type of NP that has been used to study protein adsorption. In contrast with HPMA copolymer systems, all previous publications cluster around NPs with a strong either hydrophobic or charged surface. Even the presence of PEG as a shell results in the formation of protein corona due to hydrogen bond interactions.

Conclusions

The presence of protein corona around biocompatible HPMA copolymer-based NPs was inspected by a method with the highest sensitivity to polymer chain dynamics – electron paramagnetic resonance (EPR). In contrast to previous observations, no "hard corona–soft corona" structure was observed for radical containing NPs (RNP) differing in the location of TEMPO radicals in the NP structure in the presence of HSA, IgG, low- and high-density lipoproteins, and human blood plasma itself. Our study confirms that a classical "hard corona–soft corona" paradigm is not valid for all types of NPs and each system has a unique protein corona that is determined by the nature of the NP material.

Conflicts of interest

There are no conflicts to declare.

Acknowledgements

We acknowledge financial support from the Ministry of Education, Youth and Sports of the Czech Republic (grant no. LH15213). This work was supported by the grants 17-07164S from the Czech Science Foundation and Progres Q28 from Charles University. The authors thank Dr O. Janoušková (Institute of Macromolecular Chemistry, Czech Academy of Sciences) for providing blood plasma.

Notes and references

1 E. Blanco, H. Shen and M. Ferrari, *Nat. Biotechnol.*, 2015, **33**, 941–951.
2 A. M. Jhaveri and V. P. Torchilin, *Front. Pharmacol.*, 2014, **5**, 1–26.
3 C. J. Cheng, G. T. Tietjen, J. K. Saucier-Sawyer and W. M. Saltzman, *Nat. Rev. Drug Discovery*, 2015, **14**, 239–247.
4 N. Kamaly, Z. Xiao, P. M. Valencia, A. F. Radovic-Moreno and O. C. Farokhzad, *Chem. Soc. Rev.*, 2012, **41**, 2971–3010.
5 P. Aggarwal, J. B. Hall, C. B. McLeland, M. A. Dobrovolskaia and S. E. McNeil, *Adv. Drug Delivery Rev.*, 2009, **61**, 428–437.
6 T. Cedervall, I. Lynch, S. Lindman, T. Berggård, E. Thulin, H. Nilsson, K. A. Dawson and S. Linse, *Proc. Natl. Acad. Sci. U. S. A.*, 2007, **104**, 2050–2055.
7 M. Mahmoudi, I. Lynch, M. R. Ejtehadi, M. P. Monopoli, F. B. Bombelli and S. Laurent, *Chem. Rev.*, 2011, **111**, 5610–5637.
8 Y. Kim, S. M. Ko and J.-M. Nam, *Chem. – Asian J.*, 2016, **11**, 1869–1877.
9 S. R. Saptarshi, A. Duschl and A. L. Lopata, *J. Nanobiotechnol.*, 2013, **11**, 26.
10 A. A. Shemetov, I. Nabiev and A. Sukhanova, *ACS Nano*, 2012, **6**, 4585–4602.
11 M. Rahman, S. Laurent, N. Tawil, L. Yahia and M. Mahmoudi, *Protein-Nanoparticle Interactions: The Bio-Nano Interface*, Springer, Heidelberg, New York, 2013.
12 S.-T. Yang, Y. Liu, Y.-W. Wang and A. Cao, *Small*, 2013, **9**, 1635–1653.
13 C. D. Walkey and W. C. W. Chan, *Chem. Soc. Rev.*, 2012, **41**, 2780–2799.
14 M. P. Monopoli, C. Åberg, A. Salvati and K. A. Dawson, *Nat. Nanotechnol.*, 2012, **7**, 779–786.
15 M. Lundqvist, J. Stigler, T. Cedervall, T. Berggård, M. B. Flanagan, I. Lynch, G. Elia and K. Dawson, *ACS Nano*, 2011, **5**, 7503–7509.
16 I. Lynch and K. A. Dawson, *Nano Today*, 2008, **3**, 40–47.
17 P. P. Karmali and D. Simberg, *Expert Opin. Drug Delivery*, 2011, **8**, 343–357.
18 Y. K. Lee, E.-J. Choi, T. J. Webster, S.-H. Kim and D. Khang, *Int. J. Nanomed.*, 2015, **10**, 97–113.
19 D. Walczyk, F. B. Bombelli, M. P. Monopoli, I. Lynch and K. A. Dawson, *J. Am. Chem. Soc.*, 2010, **132**, 5761–5768.
20 L. Vroman and A. L. Adams, *J. Colloid Interface Sci.*, 1986, **111**, 391–402.
21 Z. Zhu, C. Xie, Q. Liu, X. Zhen, X. Zheng, W. Wu, R. Li, Y. Ding, X. Jiang and B. Liu, *Biomaterials*, 2011, **32**, 9525–9535.
22 S. Kamei and J. Kopeček, *Pharm. Res.*, 1995, **12**, 663–668.
23 D. F. Moyano, K. Saha, G. Prakash, B. Yan, H. Kong, M. Yazdani and V. M. Rotello, *ACS Nano*, 2014, **8**, 6748–6755.
24 C. Pinholt, J. T. Bukrinsky, S. Hostrup, S. Frokjaer, W. Norde and L. Jorgensen, *Eur. J. Pharm. Biopharm.*, 2011, **77**, 139–147.
25 L. Li, Q. Mu, B. Zhang and B. Yan, *Analyst*, 2010, **135**, 1519–1530.
26 N. Li, S. Zeng, L. He and W. Zhong, *Anal. Chem.*, 2010, **82**, 7460–7466.
27 D. Bartczak, P. Vincent and H. Goenaga-Infante, *Anal. Chem.*, 2015, **87**, 5482–5485.
28 M. Hemmelmann, K. Mohr, K. Fischer, R. Zentel and M. Schmidt, *Mol. Pharm.*, 2013, **10**, 3769–3775.
29 K. Mohr, S. S. Müller, L. K. Müller, K. Rusitzka, S. Gietzen, H. Frey and M. Schmidt, *Langmuir*, 2014, **30**, 14954–14962.

30 L. Nuhn, S. Gietzen, K. Mohr, K. Fischer, K. Toh, K. Miyata, Y. Matsumoto, K. Kataoka, M. Schmidt and R. Zentel, *Biomacromolecules*, 2014, **15**, 1526–1533.
31 S. Winzen, S. Schoettler, G. Baier, C. Rosenauer, V. Mailaender, K. Landfester and K. Mohr, *Nanoscale*, 2015, **7**, 2992–3001.
32 C. D. Walkey, J. B. Olsen, F. Song, R. Liu, H. Guo, D. W. H. Olsen, Y. Cohen, A. Emili and W. C. W. Chan, *ACS Nano*, 2014, **8**, 2439–2455.
33 *Spin Labeling*, ed. L. J. Berliner and J. Reuben, Springer, US, Boston, MA, 1989, vol. 8.
34 S. Valić, M. Andreis and D. Klepac, in *Handbook of Multiphase Polymer Systems*, ed. A. Boudenne, L. Ibos, Y. Candau and S. Thomas, John Wiley & Sons, Ltd, Chichester, UK, 2011, pp. 551–584.
35 Y. Li, M. S. Budamagunta, J. Luo, W. Xiao, J. C. Voss and K. S. Lam, *ACS Nano*, 2012, **6**, 9485–9495.
36 S. Petrova, D. Klepac, R. Konefał, S. Kereïche, L. Kováčik and S. K. Filippov, *Macromolecules*, 2016, **49**, 5407–5417.
37 P. Chytil, T. Etrych, Č. Koňák, M. Šírová, T. Mrkvan, J. Bouček, B. Říhová and K. Ulbrich, *J. Controlled Release*, 2008, **127**, 121–130.
38 S. K. Filippov, P. Chytil, P. V. Konarev, M. Dyakonova, C. Papadakis, A. Zhigunov, J. Plestil, P. Stepanek, T. Etrych, K. Ulbrich and D. I. Svergun, *Biomacromolecules*, 2012, **13**, 2594–2604.
39 K. Ulbrich, V. Šubr, J. Strohalm, D. Plocová, M. Jelínková and B. Říhová, *J. Controlled Release*, 2000, **64**, 63–79.
40 V. Šubr and K. Ulbrich, *React. Funct. Polym.*, 2006, **66**, 1525–1538.
41 T. Etrych, T. Mrkvan, P. Chytil, Č. Koňák, B. Říhová and K. Ulbrich, *J. Appl. Polym. Sci.*, 2008, **109**, 3050–3061.
42 E. Lepeltier, C. Bourgaux and P. Couvreur, *Adv. Drug Delivery Rev.*, 2014, **71**, 86–97.
43 D. E. Budil, S. Lee, S. Saxena and J. H. Freed, *J. Magn. Reson., Ser. A*, 1996, **120**, 155–189.
44 J. Dubochet, M. Adrian, J.-J. Chang, J.-C. Homo, J. Lepault, A. W. McDowall and P. Schultz, *Q. Rev. Biophys.*, 1988, **21**, 129–228.
45 *Advanced ESR Methods in Polymer Research*, ed. S. Schlick, John Wiley & Sons, Inc., Hoboken, NJ, USA, 2006.
46 Z. Veksli, M. Andreis and B. Rakvin, *Prog. Polym. Sci.*, 2000, **25**, 949–986.
47 *EPR Spectroscopy: Applications in Chemistry and Biology*, ed. M. Drescher and G. Jeschke, Springer, Heidelberg, 2012.
48 S. Domingo Köhler, A. Weber, S. P. Howard, W. Welte and M. Drescher, *Protein Sci.*, 2010, **19**, 625–630.
49 J. Pilar, J. Labsky, J. Kalal and J. H. Freed, *J. Phys. Chem.*, 1979, **83**, 1907–1914.
50 A. K. Bhuyan, *Biopolymers*, 2010, **93**, 186–199.
51 N. Kang, M.-È. Perron, R. E. Prud'homme, Y. Zhang, G. Gaucher and J.-C. Leroux, *Nano Lett.*, 2005, **5**, 315–319.
52 J. V. M. Weaver, Y. Tang, S. Liu, P. D. Iddon, R. Grigg, N. C. Billingham, S. P. Armes, R. Hunter and S. P. Rannard, *Angew. Chem., Int. Ed.*, 2004, **43**, 1389–1392.
53 C. Yang, J. P. K. Tan, W. Cheng, A. B. E. Attia, C. T. Y. Ting, A. Nelson, J. L. Hedrick and Y.-Y. Yang, *Nano Today*, 2010, **5**, 515–523.
54 M. J. Joralemon, R. K. O'Reilly, C. J. Hawker and K. L. Wooley, *J. Am. Chem. Soc.*, 2005, **127**, 16892–16899.
55 E. S. Read and S. P. Armes, *Chem. Commun.*, 2007, 3021–3035.
56 M. Elsabahy and K. L. Wooley, *Chem. Soc. Rev.*, 2012, **41**, 2545–2561.
57 A. N. Koo, H. J. Lee, S. E. Kim, J. H. Chang, C. Park, C. Kim, J. H. Park and S. C. Lee, *Chem. Commun.*, 2008, 6570–6572.
58 Y. Li, K. Xiao, J. Luo, W. Xiao, J. S. Lee, A. M. Gonik, J. Kato, T. A. Dong and K. S. Lam, *Biomaterials*, 2011, **32**, 6633–6645.
59 N. L. Anderson and N. G. Anderson, *Mol. Cell. Proteomics*, 2002, **1**, 845–867.
60 S. Lewington, G. Whitlock, R. Clarke, P. Sherliker, J. Emberson, J. Halsey, N. Qizilbash, R. Peto and R. Collins, *Lancet*, 2007, **370**, 1829–1839.
61 A. Gonzalez-Quintela, R. Alende, F. Gude, J. Campos, J. Rey, L. M. Meijide, C. Fernandez-Merino and C. Vidal, *Clin. Exp. Immunol.*, 2008, **151**, 42–50.
62 G. Fanali, A. di Masi, V. Trezza, M. Marino, M. Fasano and P. Ascenzi, *Mol. Aspects Med.*, 2012, **33**, 209–290.
63 B. A. Aguilar-Castillo, J. L. Santos, H. Luo, Y. E. Aguirre-Chagala, T. Palacios-Hernández and M. Herrera-Alonso, *Soft Matter*, 2015, **11**, 7296–7307.
64 H. Wei, R.-X. Zhuo and X.-Z. Zhang, *Prog. Polym. Sci.*, 2013, **38**, 503–535.
65 Y. Li, K. Xiao, W. Zhu, W. Deng and K. S. Lam, *Adv. Drug Delivery Rev.*, 2014, **66**, 58–73.
66 K. Xiao, Y.-P. Li, C. Wang, S. Ahmad, M. Vu, K. Kuma, Y.-Q. Cheng and K. S. Lam, *Biomaterials*, 2015, **67**, 183–193.
67 R. Cukalevski, S. A. Ferreira, C. J. Dunning, T. Berggård and T. Cedervall, *Nano Res.*, 2015, **8**, 2733–2743.

